Journal of Porous Media, 20(10):921–939 (2017)

NATURAL CONVECTION IN A SQUARE CAVITY FILLED WITH A NON-DARCY POROUS MEDIUM SATURATED WITH NANOFLUID BY THE BOUNDARY ELEMENT METHOD

Janja Kramer Stajnko,[1,] Jure Ravnik,[2] & Renata Jecl[1]*

[1]*Faculty of Civil Engineering, Transportation Engineering, and Architecture, University of Maribor, Smetanova 17, SI-2000 Maribor, Slovenia*

[2]*Faculty of Mechanical Engineering, University of Maribor, Smetanova 17, SI-2000 Maribor, Slovenia*

*Address all correspondence to: Janja Kramer Stajnko, Faculty of Civil Engineering, Transportation Engineering, and Architecture, University of Maribor, Smetanova 17, SI-2000 Maribor, Slovenia; Tel.: +386 2 22 94 324, E-mail: janja.kramer@um.si

Original Manuscript Submitted: 5/18/2016; Final Draft Received: 11/8/2016

Natural convection in a differentially heated square cavity filled with nanofluid-saturated porous media is analyzed numerically using the boundary element method (BEM). The mathematical model for fluid flow through porous media is based on the Darcy–Brinkman–Forchheimer formulation; moreover, a single-phase nanofluid model was used. The coupled set of partial differential equations is solved with the numerical algorithm, which is based on the combination of single and subdomain BEM and solves the velocity–vorticity formulation of the governing equations. The simulations for different nanofluid suspensions of Cu, Al_2O_3, and TiO_2 solid nanoparticles in water as a base fluid saturating porous media were performed. The effects of solid volume fraction of nanoparticles, porosity of porous media, and various thermophysical parameters on heat transfer and fluid flow regime were investigated. The developed numerical algorithm has been validated by a comparison to available published numerical results. The addition of nanoparticles into a base fluid in saturated porous media seems to enhance the heat transfer in case of a conduction flow regime, where higher values of Nusselt numbers are observed with an increase of solid volume fraction of nanoparticles. On the other hand, the addition of nanoparticles into a base fluid diminishes the convection in porous media in case of a Darcy flow regime, which results in lower values of the Nusselt number.

KEY WORDS: *nanofluids, porous media, boundary element method, natural convection, velocity–vorticity formulation, Darcy–Brinkman–Forchheimer formulation*

1. INTRODUCTION

The use of nano-scale particles in the base fluid, also called nanofluids, is an innovative technique generally used to enhance heat transfer or cooling processes and was first introduced by Choi and Eastman (1995). Several experimental and theoretical investigations have been performed recently to analyze the effect of improved heat transfer characteristics in different configurations and applications. A comprehensive review of available studies considering convective heat transfer enhancement with nanofluids for the examples of forced convection was published by Kakaç and Pramuanjaroenkij (2009). In addition, a review of experimental and theoretical studies on natural convective heat transfer of nanofluids for different types of enclosures was published by Haddad et al. (2012). However, the role of added nanoparticles into a base fluid in natural convection heat transfer applications is still controversial, since there seem to be some discrepancies between the numerical and experimental results as reported in Abu-Nada et al. (2010) and Prabhat et al. (2012).

NOMENCLATURE

a	Ergun's constant a = 150
b	Ergun's constant b = 1.75
$c(\vec{\xi})$	geometric coefficient
c_p	specific heat at constant pressure
d_p	average particle size of the bed
Da	Darcy number
F	Forchheimer coefficient
$\vec{g}$	acceleration due to gravity
k	thermal conductivity
K	permeability of porous medium
L	characteristic length
$\vec{n}$	unit normal vector
Nu	Nusselt number
p	pressure
q	vorticity flux
q_T	temperature flux
$\vec{r}$	position vector
Pr	Prandtl number
Ra_p	porous thermal Rayleigh number; $\mathrm{Ra}_p = \mathrm{Ra}_T \cdot \mathrm{Da}$
Ra_T	fluid Rayleigh number
t	time
T	temperature
u^*	fundamental solution of the Laplace equation
V	volume
$\vec{v}$	velocity vector

Greek Symbols

α	thermal diffusivity
β	thermal expansion coefficient
Γ	boundary of the computational domain
ζ	inner angle
θ	boundary shape function
ϑ	boundary shape function for flux
Θ	domain shape function
$\vec{\xi}$	source or collocation point
φ	solid volume fraction of nanoparticles
ρ	density
μ	dynamic viscosity
ϕ	porosity
σ	specific heat ratio
$\vec{\omega}$	vorticity vector

Subscripts

0	reference (average value)
c	cold wall
f	fluid phase
h	hot wall
nf	nanofluid
p	solid phase of porous medium
s	solid phase of nanofluid

The phenomena of natural convection in fluid saturated porous media domains was investigated extensively in recent decades, mainly because it occurs in several engineering applications, such as building insulation systems, transport processes in geothermal reservoirs, pollutant transport in underground, and combustion technology, just to name a few. There exist many comprehensive studies considering the convective flow in porous media domains that may be found in books by Pop and Ingham (2001), Vafai (2005), and Nield and Bejan (2013). However, convective heat transfer of nanofluids in porous media domains is still not well investigated. A review of published articles on convection heat transfer in porous media with nanofluid was summarized by Mahdi et al. (2015).

The mathematical description of convective heat transfer with nanofluids can generally be based on a single-phase or a two-phase approach. Since the nanofluids are a two-phase mixture in general, a two-phase model seems to be more appropriate to describe the transport processes. The model predicts the interaction between the fluid and solid particles that occurs due to gravity, friction between the fluid and solid particles, Brownian forces, Brownian diffusion, sedimentation, and dispersion. There are several published articles where the behavior of nanofluids is described by a mixture theory. The most popular model for convective transport in nanofluids was proposed by Buongiorno (2006), where the nanofluid is assumed to be a two-component mixture; moreover, chemical reactions, external forces, viscous dissipation, and radiative heat transfer are neglected, while nanoparticles and base fluid are assumed to be locally in thermal equilibrium. The model predicts the Brownian motion and thermophoresis. The model was recently used for a study of nanofluid-saturated porous media by Kuznetsov and Nield (2011) and was later extended for a problem of the bioconvection in Kuznetsov (2012a,b). The simulation of natural convection in a square cavity filled with nanofluid was published by Celli (2013) and for the enclosures filled with nanofluid saturated porous media by Sheremet and Pop (2014) and Groşan et al. (2015). Moreover, the model was used for a simulation of steady double-diffusive mixed convection boundary layer flow past a vertical flat plate embedded in a nanofluid-saturated porous medium by Yasin et al. (2016).

On the other hand, the single-phase approach presumes that both the fluid phase and the particles are in thermal equilibrium and have the same local velocities. This is possible due to very small particle sizes ($<$ 1–100 nm) and usually low concentrations of nanoparticles (2.5%–5%), which is already enough to considerably improve the heat transfer rate of the fluids. These assumptions enable the solid–liquid mixture to be considered as a conventional single-phase fluid, where its properties, for example, density, specific heat, thermal conductivity, and viscosity, are modified according to the applied nanoparticles. A single-phase nanofluid mathematical model was proposed by Tiwari and Das (2007) and was recently used for porous media applications by Sheikhzadeh and Nazari (2013), Mittal et al. (2013), Mansour et al. (2013), Bourantas et al. (2014), Sheremet et al. (2015), Ghalambaz et al. (2015), Nguyen et al. (2015), and Saleh and Hashim (2015).

In the present study, the natural convection in a two-dimensional porous cavity saturated with nanofluid and differentially heated is analyzed to determine the influence of different types of added nanoparticles and concentrations on the heat transfer. The single-phase nanofluid mathematical model was used as proposed in Tiwari and Das (2007) and Nguyen et al. (2015) with the Darcy–Brinkman–Forchheimer momentum equation for the porous media flow. A novel numerical approach based on the BEM has been used to solve the governing set of partial differential equations. Therefore the velocity–vorticity formulation of the governing equations has been employed, as proposed in Ravnik et al. (2010). The unknown field functions are solved using the combination of single-domain and subdomain BEM. The boundary vorticity values are obtained from the kinematics equation by a singe-domain BEM (Škerget and Jecl, 2003), while the domain vorticity, velocity, and temperature values are solved by a subdomain BEM (Ramšak et al., 2005). The influence of nanoparticles and porous matrix on the heat transfer and fluid flow characteristics is analyzed.

2. PROBLEM FORMULATION

The problem under consideration is a two-dimensional square cavity which is considered to be filled with a porous medium and fully saturated with nanofluid, shown in Fig. 1, where x and y are Cartesian coordinates and L is the length and height of the cavity. Horizontal walls are considered to be adiabatic ($\partial T/\partial y = 0$), where T is temperature, while vertical walls are differentially heated with constant temperatures T_h on the hot wall and T_c on the cold wall. Owing to the temperature difference between the vertical walls, the density of the fluid changes, resulting in buoyancy forces, which induce convective motion. The fluid rises along the hot wall and begins to transport heat toward the cold

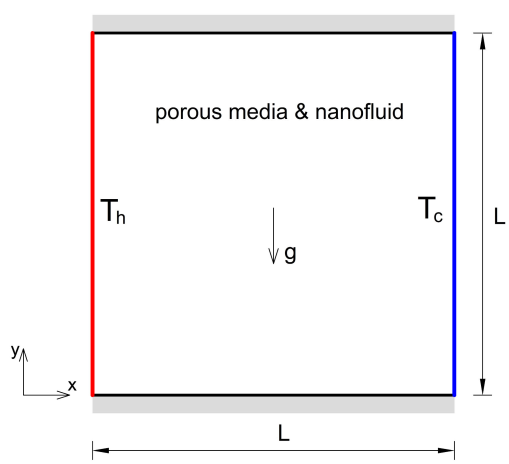

FIG. 1: Computational domain with boundary conditions

wall. The heat flux depends on the type of the fluid, the type and amount of added nanoparticles, and permeability of porous media.

The porous medium is assumed to be isotropic, homogenous, and in thermal equilibrium with the fluid phase, which is a suspension of water and nanoparticles. Three different types of solid spherical nanoparticles were considered, namely, the Cu, Al_2O_3, and TiO_2. The thermophysical properties of nanofluid are given with density ρ_{nf}, dynamic viscosity μ_{nf}, heat capacitance $(c_p)_{nf}$, thermal expansion coefficient β_{nf}, and thermal conductivity k_{nf}, where index nf stands for the nanofluid. All nanofluid properties are given with relationships to pure fluid and pure solid properties, linked with solid volume fraction of nanoparticles φ, given as:

$$\varphi = \frac{V_s}{V_s + V_f} \tag{1}$$

where V_s is volume of solid particles and V_f is volume of fluid. The expressions for thermophysical properties of nanofluid are reviewed in Haddad et al. (2012) and are listed below, where the index f stands for the fluid phase and s for the solid phase:

Effective Density of Nanofluid ρ_{nf}:

$$\rho_{nf} = (1 - \varphi)\rho_f + \varphi\rho_s \tag{2}$$

Effective Dynamic Viscosity μ_{nf}, Brinkman Model (Brinkman, 1952):

$$\mu_{nf} = \frac{\mu_f}{(1 - \varphi)^{2.5}} \tag{3}$$

Heat Capacitance $(c_p)_{nf}$:

$$(\rho c_p)_{nf} = (1 - \varphi)(\rho c_p)_f + \varphi(\rho c_p)_s \tag{4}$$

Thermal Expansion Coefficient β_{nf}:

$$(\rho\beta)_{nf} = (1 - \varphi)(\rho\beta)_f + \varphi(\rho\beta)_s \tag{5}$$

Effective Thermal Conductivity k_{nf}, Wasp Model (Wasp, 1977):

$$k_{nf} = k_f \frac{k_s + 2k_f - 2\varphi(k_f - k_s)}{k_s + 2k_f + \varphi(k_f - k_s)} \tag{6}$$

The thermophysical properties of base fluid and, in this study, used nanoparticles are given in Table 1.

It is further assumed that the nanoparticles are in thermal equilibrium with the base fluid and the nonslip boundary condition is considered. The fluid flow is assumed to be laminar, steady, Newtonian, and incompressible, where the density depends only on the temperature variations, which can be taken into account with the Boussinesq approximation as:

$$\rho_{nf} = \rho_0(1 - \beta_{nf}(T - T_0)) \tag{7}$$

where index 0 refers to a reference state.

TABLE 1: Thermophysical properties of water and Cu, Al_2O_3, and TiO_2 solid nanoparticles (adapted from Oztop and Abu-Nada, 2008)

	Water	Cu	Al_2O_3	TiO_2
c_p [J/kgK]	4179	385	795	686.2
ρ [kg/m^3]	997.1	8933	3970	4250
k [W/mK]	0.613	400	40	8.9538
β [$\times 10^{-5}$ K^{-1}]	21	1.67	0.85	0.9
α [$\times 10^{-7}$ m^2/s]	1.47	1163	131.7	30.7

2.1 Mathematical Model

The mathematical model for heat transfer of nanofluids in porous media is based on the conservation equations for mass, momentum, and energy, which are obtained from the Navier–Stokes equations, generally written at the microscopic level for pure fluid flow. Since the geometry of porous media is irregular and complex in general, microscopic description is not appropriate for a fluid flow model. Consequently, all equations are averaged over the representative elementary volume (REV), where only one part of the computational domain is available for the fluid flow. All details about the averaging procedure are given in Bear (1972) and are omitted in this article.

The general set of governing equations describing nanofluid flow in porous media can thus be written at the macroscopic level as follows:

- Continuity Equation:

$$\vec{\nabla} \cdot \vec{v} = 0 \tag{8}$$

- Momentum Equation:

$$\frac{1}{\phi}\frac{\partial \vec{v}}{\partial t} + \frac{1}{\phi^2}(\vec{v}\cdot\vec{\nabla})\vec{v} = -\frac{1}{\rho_{nf}}\vec{\nabla}p - \beta_{nf}(T-T_0)\vec{g} + \frac{1}{\phi}\frac{\mu_{nf}}{\rho_{nf}}\nabla^2\vec{v} - \frac{1}{K}\frac{\mu_{nf}}{\rho_{nf}}\vec{v} - \frac{F\vec{v}|\vec{v}|}{K^{1/2}} \tag{9}$$

- Energy Equation:

$$\sigma\frac{\partial T}{\partial t} + (\vec{v}\cdot\vec{\nabla})T = \frac{k_{enf}}{(\rho c_p)_{nf}}\nabla^2 T \tag{10}$$

The parameters in the preceding equations are $\vec{v}$ volume averaged velocity vector, ϕ porosity, t time, p fluid pressure, T temperature, $\vec{g}$ gravitational acceleration, K permeability, and F Forchheimer coefficient. In the energy equation, σ is specific heat ratio $\sigma = \phi + (1-\phi)(\rho c_p)_p/(\rho c_p)_{nf}$, where $(\rho c_p)_p$ and $(\rho c_p)_{nf}$ are heat capacitances of solid and fluid phase, respectively; moreover, k_{enf} is the effective conductivity of the nanofluid-saturated porous medium as given in Sheremet et al. (2015):

$$k_{enf} = \phi k_{nf} + (1-\phi)k_p = k_e\left\{1 - \frac{2\phi k_f(k_f-k_s)}{k_e\left[k_s + 2k_f + \varphi(k_f-k_s)\right]}\right\} \tag{11}$$

where k_e is the effective thermal conductivity of the clear fluid-saturated porous medium $k_e = \phi k_f + (1-\phi)k_s$, k_f is thermal conductivity of the clear fluid, and k_s is thermal conductivity of (nano) particles.

In this study, the thermal properties of the solid matrix and the nanofluid are considered to be identical, resulting in $\sigma = 1$ (Nguyen et al., 2015). Furthermore, the effective conductivity of the nanofluid saturated porous medium k_{enf} is assumed to be equal to the thermal conductivity of the nanofluid k_{nf} according to the assumptions in Bourantas et al. (2014).

The momentum Eq. (9), also known as the Brinkman–Forchheimer equation, consists of two viscous and two inertia terms. The last three terms on the r.h.s. of the equation represent the Brinkman viscous term, the Darcy term, and the Forchhemer inertia term, which describe nonlinear influences at higher velocities. The Forchheimer coefficient or dimensionless form-drag constant varies with the nature of the porous medium and can be written according to the Ergun model as proposed in Nield and Bejan (2013):

$$K = \frac{\phi^3 d_p^2}{a(1-\phi)^2}, \quad F = \frac{b}{\sqrt{a\phi^3}} \tag{12}$$

where a and b are Ergun's constants with values a = 150 and b = 1.75 (Ergun, 1952) and d_p is the average particle size of the bed. The following dimensionless variables are employed to convert Eqs. (8), (9), and (10) into nondimensional form:

$$\vec{v} \to \frac{\vec{v}}{v_0}, \quad \vec{r} \to \frac{\vec{r}}{L}, \quad t \to \frac{v_0 t}{L}, \quad \vec{g} \to \frac{\vec{g}}{g_0}, \quad p \to \frac{p}{p_0}, \quad T \to \frac{(T-T_0)}{\Delta T} \tag{13}$$

where v_0 is characteristic velocity given with an expression $v_0 = k_f/(\rho c_p)_f L$, k_f is pure fluid thermal conductivity, $(\rho c_p)_f$ is heat capacity for the pure fluid phase, and L is characteristic length (e.g., length of one side of the square cavity). Moreover, T_0 is characteristic temperature $T_0 = (T_2 - T_1)/2$, where ΔT is characteristic temperature difference $\Delta T = T_2 - T_1$, p_0 is characteristic pressure p_0 = 1 bar, and gravitational acceleration is g_0 = 9.81 m/s^2.

Furthermore, the velocity–vorticity formulation is proposed by defining the vorticity vector as a curl of the velocity field $\vec{\omega} = \vec{\nabla} \times \vec{v}$. The governing set of equations is thus transformed into the following form:

$$\nabla^2 \vec{v} + \vec{\nabla} \times \vec{\omega} = 0 \tag{14}$$

$$(\vec{v} \cdot \vec{\nabla})\vec{\omega} = (\vec{\omega} \cdot \vec{\nabla})\vec{v} - \mathrm{PrRa}_T \phi^2 \frac{\beta_{nf}}{\beta_f} \vec{\nabla} \times T\vec{g} + \mathrm{Pr}\phi \frac{\mu_{nf}}{\mu_f} \frac{\rho_f}{\rho_{nf}} \nabla^2 \vec{\omega} - \frac{\mathrm{Pr}}{\mathrm{Da}} \phi^2 \frac{\mu_{nf}}{\mu_f} \frac{\rho_f}{\rho_{nf}} \vec{\omega} - \frac{F}{\sqrt{\mathrm{Da}}} \phi^2 |\vec{v}| \vec{\omega} \tag{15}$$

$$(\vec{v} \cdot \vec{\nabla}) T = \frac{\alpha_{nf}}{\alpha_f} \nabla^2 T \tag{16}$$

where α_{nf} is thermal diffusivity of nanofluid $\alpha_{nf} = k_{nf}/(\rho c_p)_{nf}$ and α_f is thermal diffusivity of pure fluid $\alpha_f = k_f/(\rho c_p)_f$. Since, in this study, only steady flow fields are considered, the time derivatives in the vorticity and energy equations, $\partial\vec{\omega}/\partial t$, $\partial T/\partial t$, are omitted. The governing nondimensional parameters for the present problem are as follows:

- Fluid Rayleigh number Ra$_T$ = $g\beta_T \Delta T L^3 \rho_f (\rho c_p)_f / \mu_f k_f$
- Darcy number Da = K/L^2
- Porous Rayleigh number Ra$_p$ = Ra$_T \cdot$ Da
- Prandtl number Pr = $\mu_f c_p / k_f$
- Darcy number Da = K/L^2
- Porosity ϕ

The boundary conditions for the current two-dimensional problem are

$$\begin{array}{llll} v_x = v_y = 0, & \omega = 0, & T = T_h & \text{at} \quad x = 0, \quad 0 \le y \le 1 \\ v_x = v_y = 0, & \omega = 0, & T = T_c & \text{at} \quad x = L, \quad 0 \le y \le 1 \\ v_x = v_y = 0, & \omega = 0, & \dfrac{\partial T}{\partial y} = 0 & \text{at} \quad y = 0, \quad 0 \le x \le 1 \\ v_x = v_y = 0, & \omega = 0, & \dfrac{\partial T}{\partial y} = 0 & \text{at} \quad y = L, \quad 0 \le x \le 1 \end{array} \tag{17}$$

The wall heat flux is calculated to determine the overall heat transfer of nanofluids through porous media, which is expressed with the average Nusselt number and can be written for the case of nanofluids as

$$\mathrm{Nu} = \frac{k_{nf}}{k_f} \int_\Gamma \vec{\nabla} T \cdot \vec{n} d\Gamma \tag{18}$$

where Γ is the surface through which the heat flux is calculated and $\vec{n}$ is a unit normal to this surface.

3. NUMERICAL METHOD

The governing set of Eqs. (14), (15), and (16) is solved using an algorithm based on the BEM which solves the velocity–vorticity formulation of Navier–Stokes equations by a combination of single and subdomain BEM and was first developed for pure fluid flow simulations by Ravnik et al. (2008, 2009). Furthermore, the solver has been adapted for porous media flow simulations by Kramer et al. (2011, 2013) and upgraded by inclusion of nanofluid properties for simulation of flow and heat transfer of nanofluids (Ravnik et al., 2010). For purposes of this study, additional parameters describing nanofluid properties together with porous media flow characteristics have been included in the solver to simulate flow and heat transfer of nanofluid saturated porous media.

The algorithm requires known boundary conditions for velocity and temperature either of Dirichlet or Neumann type, given with expressions (17). On all solid walls, the no-slip boundary conditions are prescribed in addition to temperature or temperature flux. The boundary conditions for the vorticity are unknown at the beginning and are calculated as a part of the numerical algorithm. This is not entirely true, since a problem with non-slip velocity boundary conditions on all walls is considered, consequently, the vorticity is $\omega = 0$.

In the first step, a single-domain BEM is used on the kinematics equation (14) to calculate the boundary vorticity values. The kinematic equation (14) is used again to calculate the domain velocity values by a subdomain BEM. The domain temperature values are calculated out of Eq. (16) using a subdomain BEM, and finally, the domain vorticity values are obtained out of vorticity transport equation (15) using the subdomain BEM. At the end of each iteration, the convergence criterion is checked, which is calculated as the RMS difference between the field functions of current and previous iterations. The iteration is stopped when the RMS difference for all field functions is less than 10^{-5}. To achieve convergence, underrelaxation of vorticity and temperature values ranging from 0.1 to 0.01 is used.

All governing equations are written in the integral form, which is done using Green's second identity for the unknown field function and known fundamental solution u^* of the diffusion operator, $u^* = 1/4\pi|\vec{\xi} - \vec{r}|$, where $\vec{\xi}$ is a source or collocation point on the boundary Γ and $\vec{r}$ is an integration point in the domain Ω. The integral representation of the kinematic equation in its tangential form as proposed in Ravnik et al. (2008) and Žunič et al. (2007) is given with

$$c(\vec{\xi})\vec{n}(\vec{\xi}) \times \vec{v}(\vec{\xi}) + \vec{n}(\vec{\xi}) \times \int_\Gamma \vec{v}\;\vec{\nabla}u^* \cdot \vec{n}d\Gamma = \vec{n}(\vec{\xi}) \times \int_\Gamma \vec{v} \times (\vec{n} \times \vec{\nabla})u^* d\Gamma + \vec{n}(\vec{\xi}) \times \int_\Omega (\vec{\omega} \times \vec{\nabla}u^*)d\Omega \tag{19}$$

where $c(\vec{\xi})$ is the geometric coefficient given as $c(\xi) = \zeta/4\pi$ and ζ is the inner angle with origin in $\vec{\xi}$. The boundary vorticity values are calculated from the tangential form of the kinematics equation.

3.1 Subdomain BEM Solution of the Vorticity and Energy Transport Equations

The domain vorticity and temperature values are calculated out of Eqs. (15) and (16) by a subdomain BEM, where the boundary vorticity values obtained by the single domain BEM are used as Dirichlet boundary conditions in the vorticity equation, while the temperature boundary conditions of Dirichlet or Neumann type are prescribed by the user. The boundary-domain integral forms of the vorticity and energy transport equations are

$$\begin{aligned} c(\vec{\xi})\omega_j(\vec{\xi}) + \int_\Gamma \omega_j \vec{\nabla}u^* \cdot \vec{n}d\Gamma = \int_\Gamma u^* q_j d\Gamma + \frac{1}{\phi}\frac{1}{\mathrm{Pr}}\frac{\mu_f}{\mu_{nf}}\frac{\rho_{nf}}{\rho_f} \cdot \left[\int_\Gamma \vec{n} \cdot \{u^*(\vec{v}\omega_j - \vec{\omega}v_j)\}d\Gamma\right. \\ \left. - \int_\Omega (\vec{v}\omega_j - \vec{\omega}v_j) \cdot \vec{\nabla}u^* d\Omega\right] - \phi\mathrm{Ra}\frac{\beta_{nf}}{\beta_f}\frac{\mu_f}{\mu_{nf}}\frac{\rho_{nf}}{\rho_f}\left[\int_\Gamma (u^* T\vec{g} \times \vec{n})_j d\Gamma\right. \\ \left. + \int_\Omega (T\vec{\nabla} \times u^*\vec{g})d\Omega\right] + \phi\frac{1}{\mathrm{Da}}\int_\Omega \vec{\omega}u^* d\Omega + \phi\frac{F}{\sqrt{\mathrm{Da}}}\frac{1}{\mathrm{Pr}}\frac{\mu_f}{\mu_{nf}}\frac{\rho_{nf}}{\rho_f}|\vec{v}|\int_\Omega \vec{\omega}u^* d\Omega, \end{aligned} \tag{20}$$

$$c(\vec{\xi})T(\vec{\xi}) + \int_\Gamma T\vec{\nabla}u^*\vec{n}d\Gamma = \int_\Gamma q_T u^* d\Gamma + \frac{k_f}{k_{nf}}\frac{(\rho c_p)_{nf}}{(\rho c_p)_f}\left[\int_\Gamma \vec{n}(u^*\vec{v}T)d\Gamma - \int_\Omega (\vec{v}T)\vec{\nabla}u^* d\Omega\right] \tag{21}$$

where q_j is the jth component of vorticity flux and q_T is the temperature flux.

To write a discrete form of the preceding equations, the domain Ω is divided into mesh elements that is, subdomains. In this work, hexahedral mesh elements are used. The field functions as well as the products of velocity and vorticity field and velocity and temperature field are interpolated within each subdomain using standard shape functions for a 27-node Lagrangian domain element. Within each hexahedron, a quadratic interpolation of function is employed, $\omega_j = \Sigma_{i=1}^{27}\Theta_i\omega_j^i$ and $T = \Sigma_{i=1}^{27}\Theta_i T^i$. On each face of the hexahedron, continuous quadratic interpolations for functions $\omega_j = \Sigma_{i=1}^{9}\theta_i\omega_j^i$ and $T = \Sigma_{i=1}^{9}\theta_i T^i$ are used, where ω_j^i and T^i are function values in each function node. Flux over the boundary element is interpolated using discontinuous linear interpolation with four nodes as $q_j = \Sigma_{i=1}^{4} \vartheta_i q_j^i$ and $q_T = \Sigma_{i=1}^{4} \vartheta_i q_T^i$.

3.2 Subdomain BEM Solution of the Velocity Equation

The domain velocity values are obtained out of the velocity equation (14) by subdomain BEM using the following integral expression:

$$c(\vec{\xi})\vec{v}(\vec{\xi}) + \int_\Gamma \vec{v}(\vec{n} \cdot \vec{\nabla} u^*) d\Gamma = \int_\Gamma \vec{v} \times (\vec{n} \times \vec{\nabla} u^*) d\Gamma + \int_\Omega (\vec{\omega} \times \vec{\nabla} u^*) d\Omega. \tag{22}$$

The boundary conditions of Dirichlet type are prescribed on the boundary of the domain, and finally, for each of the subdomains, a discrete system of linear equations is written.

4. VALIDATION TESTS

To obtain a grid-independent solution, at the beginning, a grid sensitivity analysis was performed. Four different nonuniform grids of 21 × 21, 41 × 41, 61 × 61, and 81 × 81 were tested for Cu-water nanofluid at Ra_p = 1000, Pr = 6.2, Da = 10^{-2}, 10^{-4}, and 10^{-6}, ϕ = 0.4, and φ = 0.05. The results of average Nusselt number are shown in Table 2. On the basis of the grid independence test, the nonuniform grid 41 × 41 has been used for the following analysis.

The validation of the present numerical code was carried out for the natural convection benchmark problem in a porous cavity saturated by a pure fluid with differentially heated sidewalls. The results for Pr = 1.0 and several different governing parameters (Ra_p, Da, ϕ) were compared to studies of Nithiarasu et al. (1997), and Nguyen et al. (2015) and, furthermore, for the case of small Darcy number (Da = 10^{-6}), with Lauriat and Prasad (1989). Comparison of Nusselt number values is presented in Table 3. First, the overall heat transfer was obtained from a Brinkman model [without the last term in Eq. (9)]. Moreover, the Forchheimer term was added into the momentum equation for the sake of comparison with the reference studies. A good agreement between the present and published results can be observed. However, the Nu number values obtained by the Brinkman model are slightly higher in comparison to those obtained by the Forchheimer model, where the inertial effects are additionally taken into account and which obviously reduce the heat transfer rate, as also reported in Lauriat and Prasad (1989). The influence of inertia effects seem to be predominant in the case of high Ra_p numbers and low Da, where higher deviation between the results obtained by different models can be observed. A slight discrepancy between the reference results can be observed at small values of Da. However, when comparing the results with the study of Lauriat and Prasad (1989), where, among others, the Forchheimer extension is used, the Nusselt number values in this range of Da seem to be in better agreement.

Furthermore, the proposed numerical code was validated with the results for the case of a porous cavity fully saturated with nanofluid, published by Nguyen et al. (2015), where the Cu nanoparticles were added to the water as a base fluid. The comparison of average Nu is presented in Table 4 for Pr = 6.2, different solid volume fractions of nanoparticles (φ = 0.0, 0.025, 0.05), and other governing parameters (Ra_p, Da, ϕ). Present results are obtained with the Forchheimer model. It can be observed that the results agree well with the data from the published study.

TABLE 2: Nusselt number values for different grid sizes

	Da		
Nonuniform Grid	**10^{-2}**	**10^{-4}**	**10^{-6}**
21 × 21	3.416	9.076	13.185
41 × 41	3.400	9.132	12.991
61 × 61	3.401	9.132	12.992
81 × 81	3.400	9.131	12.991

TABLE 3: Validation of the numerical code by a comparison of average Nu for natural convection in porous media saturated with a pure fluid (Pr = 1.0) for different governing parameters, with Nithiarasu et al. (1997), Nguyen et al. (2015), and Lauriat and Prasad (1989)

Da	Ra_p	Nithiarasu et al. (1997)	Nguyen et al. (2015)	Lauriat and Prasad (1989)	Present Bm	Present Fm
		ϕ = 0.4				
10^{-2}	10	1.010	1.005	—	1.007	1.008
	100	1.408	1.404	—	1.407	1.371
	1000	2.983	3.159	—	3.072	3.049
10^{-4}	10	1.067	1.062	—	1.067	1.067
	100	2.550	2.702	—	2.750	2.671
	1000	7.810	8.903	—	9.079	8.377
10^{-6}	10	1.079	1.072	1.07	1.092	1.092
	100	2.970	2.975	3.07	3.244	3.224
	1000	11.460	11.892	12.80	13.414	12.519
		ϕ = 0.6				
10^{-2}	10	1.015	1.010	—	1.012	1.012
	100	1.530	1.533	—	1.536	1.503
	1000	3.555	3.602	—	3.559	3.499
10^{-4}	10	1.071	1.065	—	1.070	1.070
	100	2.725	2.764	—	2.827	2.777
	1000	9.183	9.454	—	9.741	9.174
10^{-6}	10	1.079	1.072	—	1.093	1.093
	100	2.997	2.980	—	3.252	3.241
	1000	11.790	11.924	—	13.490	12.895
		ϕ = 0.9				
10^{-2}	10	1.020	1.015	—	1.017	1.017
	100	1.640	1.667	—	1.671	1.643
	1000	3.910	4.075	—	4.046	3.980
10^{-4}	10	1.070	1.066	—	1.073	1.073
	100	2.740	2.817	—	2.897	2.867
	1000	9.200	9.947	—	10.349	9.917
10^{-6}	10	1.080	1.072	1.07	1.093	1.093
	100	3.000	2.986	3.09	3.258	3.252
	1000	12.010	12.069	13.29	13.536	13.164

Note: Bm are results obtained by a Brinkman model and Fm results obtained by a Forchheimer model.

5. RESULTS

Figure 2 shows isotherms for Cu-water nanofluid under different values of the porous Rayleigh number and Darcy number at porosity ϕ = 0.4 and different values of solid volume fraction. Solid lines correspond to φ = 0.0, dotted lines to φ = 0.025, and dashed lines to φ = 0.05. Heat transfer in a porous medium is mostly affected by Rayleigh and Darcy numbers. At $Ra_p = 10$, the heat transfer in the horizontal direction is weak, and the main heat transfer mechanism in this case is conduction. An increase of Ra_p results in stronger convective motion, which is clearly evident from the temperature field; when $Ra_p = 1000$, thin boundary layers are created near the hot and cold walls, and the isotherms in the core region become almost horizontal and parallel to adiabatic and impermeable walls. According to the temperature fields, a decrease of Da enhances the heat transfer through the cavity. The Da number

TABLE 4: Validation of the numerical code by a comparison of average Nu for natural convection in porous media saturated with a nanofluid (Pr = 6.2) for different governing parameters with Nguyen et al. (2015)

		φ = 0.05					
		ϕ = 0.4		**ϕ = 0.6**		**ϕ = 0.9**	
Da	Ra_p	Nguyen et al. (2015)	Present	Nguyen et al. (2015)	Present	Nguyen et al. (2015)	Present
10^{-2}	1000	3.433	3.400	3.850	3.826	4.162	4.145
10^{-4}	1000	9.117	9.132	9.590	9.743	9.901	10.154
10^{-6}	1000	11.778	12.991	11.899	13.128	11.976	13.195
		ϕ = 0.4					
		φ = 0.0		**φ = 0.025**		**φ = 0.05**	
10^{-2}	10	1.007	1.008	1.081	1.083	1.160	1.162
10^{-2}	1000	3.302	3.282	3.370	3.345	3.433	3.400
10^{-6}	1000	11.867	13.238	11.847	13.131	11.778	12.991

influences the magnitude of the Darcy term in Eq. (15). When Da is increasing, the flow regime, is transited into the Darcy flow regime and the model is near to Darcy's law.

However, the addition of the nanoparticles into the base fluid results in an attenuation of the convective motion inside the porous cavity but the overall heat transfer remains the same, since the main convective cell with upward flows along the hot wall and downward flows along the cold wall is conserved.

From the results in Table 5, it is evident that overall heat transfer is enhanced with an increase of solid volume fraction of nanoparticles in case of the conduction-dominated regime (at low values of Ra_p and Da = 10^{-2}). The highest values of Nu can be observed in case of added Cu nanoparticles. In the case of a convection-dominated regime ($Ra_p \geq 100$ and Da $\leq 10^{-4}$), the addition of nanoparticles diminishes the convection, which results in lower values of Nu. The same behavior can be observed for all different types of nanoparticles.

Further computations have been carried out for several values of governing parameters: solid volume fraction of nanoparticles (φ = 0.0, 0.025, and 0.05), the porosity of the porous medium (ϕ = 0.4, 0.6, and 0.8), porous Rayleigh number (Ra_p = 10, 100, and 1000), and Darcy number (Da = 10^{-6}–10^{-1}). The water as a base fluid where Pr = 6.2, with addition of different types of nanoparticles, namely, Cu, Al_2O_3, and TiO_2, was considered in the study. To ensure the nanofluid mixture is homogenous, the solid volume fraction is considered up to 5%, since a higher concentration may cause sedimentation or absorption of particles on the solid surfaces of the porous matrix, as reported in Muthtamilselvan et al. (2010).

Figure 3 presents streamlines for Cu-water nanofluid under different values of the porous Rayleigh number and Darcy number at porosity ϕ = 0.4 and solid volume fraction φ = 0.05. The flow field consists of a single circulation flow in the clockwise direction for all different values of Ra_p and Da as a result of the applied horizontal temperature difference. With an increase of Ra_p and a decrease of Da, the circulation becomes extended along the horizontal axis; furthermore, the boundary layers become more significant.

Figure 4 shows the dependance of solid volume fraction on the average heat transfer for Cu-water nanofluid and various porous Rayleigh and Darcy numbers. In the case when conduction is is dominant heat transfer mechanism, Da = 10^{-2} [Fig. 4(a)], the heat transfer enhancement due to an increase of solid volume fraction is more evident. The addition of nanoparticles in the base fluid enhances the thermal conductivity, which consequently results in higher values of the Nusselt number. Moreover, the average Nu increases with an increase of Ra_p. With a decrease of Darcy number, Da $\leq 10^{-4}$ [Figs. 4(b) and 4(c)], when convection becomes the dominant heat transfer mechanism, it appears that average Nusselt number decreases with the solid volume fraction φ. The addition of nanoparticles in general suppresses the convection, so at this stage, further enhancement of the heat transfer rate is limited. At fixed Ra_p = 1000 [Fig. 4(d)], it is obvious that an increase of the solid volume fraction leads to a higher average Nu when Da = 10^{-2}; however, at low values of Da, average Nu decreases along with φ.

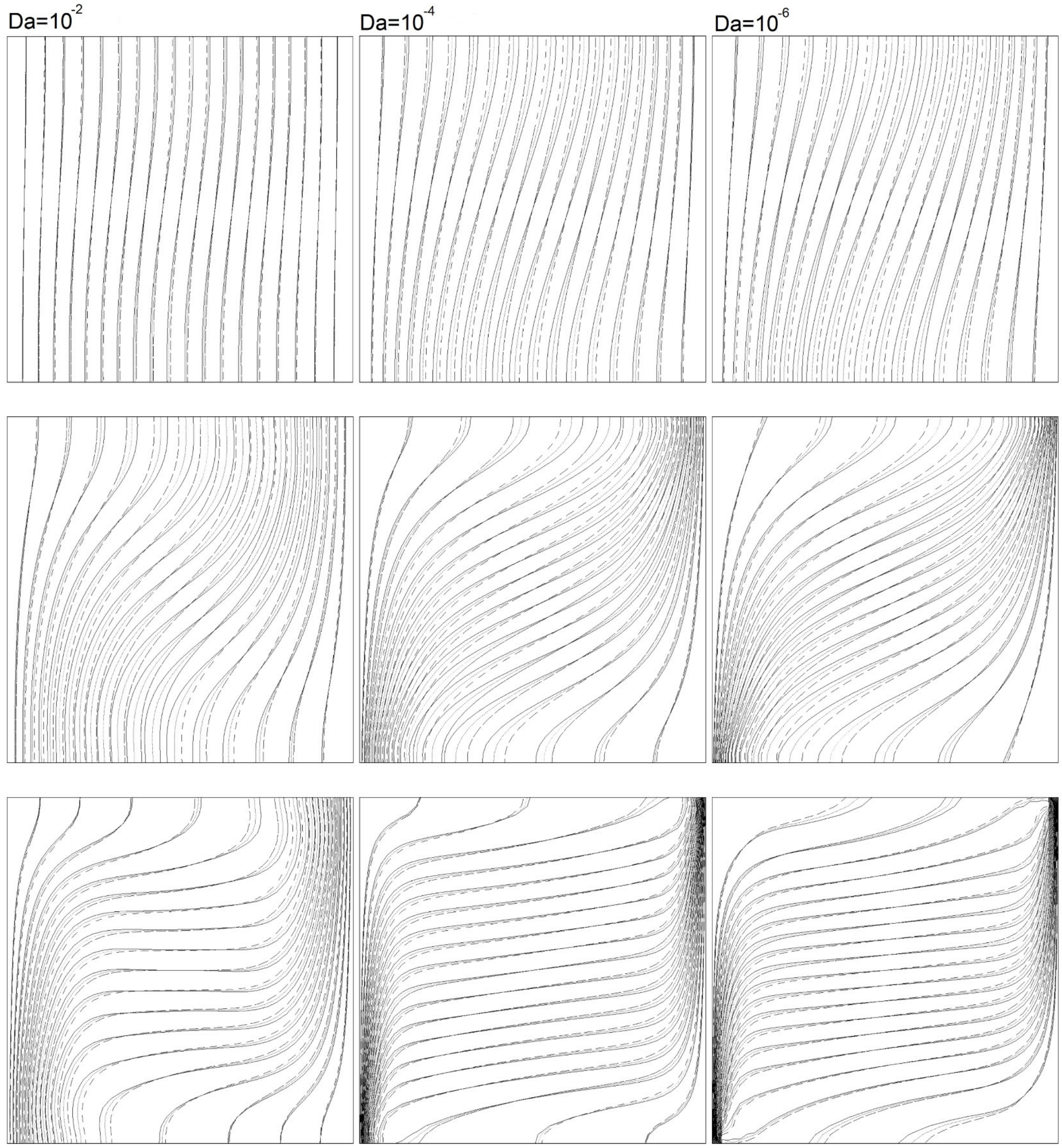

FIG. 2: Temperature contour plots for ϕ = 0.4, Ra_p = 10 (upper row), Ra_p = 100 (middle row), Ra_p = 1000 (bottom row), and various Da; solid lines φ = 0.0, dotted lines φ = 0.025, dashed lines φ = 0.05

The influence of different type of nanoparticles on average Nu at fixed $Ra_p = 1000$ and various Da is shown in Fig. 5. In the case of the conduction-dominant regime, Da = 10^{-2} [Fig. 5(a)], it is obvious that the heat transfer is enhanced due to all different types of added nanoparticles. Most efficient seem to be the Cu nanoparticles, since the heat transfer rate in that case is the highest. When Da = 10^{-4}, the addition of Cu nanoparticles still results in higher values of average Nu, while the addition of Al_2O_3 and TiO_2 suppresses the convection, resulting in lower values of Nu. At low values of Da [Fig. 5(c)], the addition of all different kinds of nanoparticles results in lower values of average Nu.

Figure 6 presents the effect of porosity ϕ and solid volume fraction φ on the average Nusselt number for Cu-water nanofluid at $Ra_p = 1000$ and various Darcy numbers. In general, the heat transfer is enhanced with an increase

TABLE 5: Nusselt number values for ϕ = 0.4 and various Ra_p, Da, φ and different types of nanofluids

Da	Ra_p	φ	Nu: Cu	Nu: Al_2O_3	Nu: TiO_2	
10^{-2}	10	0.0	1.008	1.008	1.008	
		0.025	1.083	1.081	1.069	↓
		0.05	1.162	1.155	1.133	
10^{-4}	10	0.0	1.067	1.067	1.067	
		0.025	1.131	1.128	1.116	↓
		0.05	1.201	1.192	1.171	
10^{-6}	10	0.0	1.092	1.092	1.092	
		0.025	1.152	1.148	1.137	↓
		0.05	1.218	1.208	1.187	
10^{-2}	100	0.0	1.403	1.403	1.403	
		0.025	1.437	1.429	1.418	↓
		0.05	1.475	1.456	1.436	
10^{-4}	100	0.0	2.736	2.736	2.736	
		0.025	2.695	2.671	2.657	↑
		0.05	2.653	2.599	2.577	
10^{-6}	100	0.0	3.240	3.240	3.240	
		0.025	3.160	3.127	3.113	↑
		0.05	3.080	3.009	2.988	
10^{-2}	1000	0.0	3.282	3.282	3.282	
		0.025	3.345	3.328	3.303	↓
		0.05	3.400	3.359	3.317	
10^{-4}	1000	0.0	9.072	9.072	9.072	
		0.025	9.115	9.063	9.002	↑
		0.05	9.132	9.003	8.908	
10^{-6}	1000	0.0	13.238	13.238	13.238	
		0.025	13.131	13.032	12.957	↑
		0.05	12.991	12.756	12.642	

of porosity, which is specially obvious at high values of Da [Fig. 6(a)]. With a decrease of Da, the addition of nanoparticles starts to slow down the convective motion, which results in lower values of Nu, as clearly shown in Figs. 6(b), 6(c), and 6(d).

In Figs. 7, 8, 9, and 10 temperature and velocity profiles at the horizontal midsection of the cavity are shown. Figure 7 presents the dependence of temperature and velocity gradients on the Ra_p at Da = 10^{-4}. Higher temperature gradients can be observed at higher values of Ra_p; moreover, the velocity profile seems to have peaks near to the vertical walls. However, when Ra_p = 10, the temperature profile is almost linear, indicating the pure conduction regime, which can also be clearly observed from the velocity profile. The dependance on the Da number at Ra_p = 1000, ϕ = 0.4, and φ = 0.05 is shown in Fig. 8. In the case of a Darcy flow regime (Da = 10^{-6}), the highest temperature

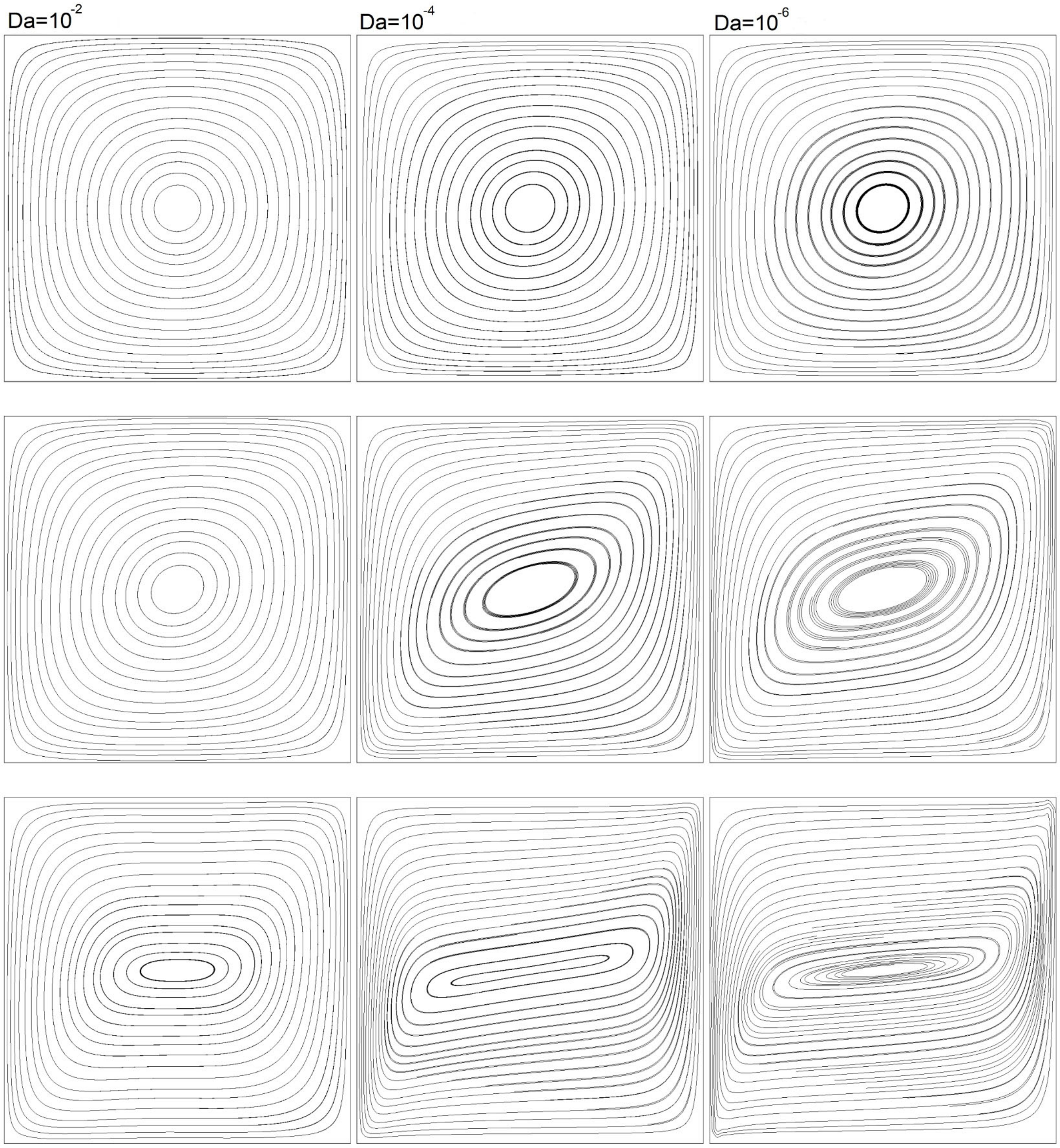

FIG. 3: Streamlines for ϕ = 0.4, φ = 0.05, and Ra_p = 10 (upper row), Ra_p = 100 (middle row), Ra_p = 1000 (bottom row), and various Da

and velocity gradients can be observed, while the maximum and minimum values of velocity can be found near to the vertical walls as a typical characteristic for the pure Darcy flow. The temperature profile seems to be similar for the transition regime at Da = 10^{-4}. With an increase of Da toward a non-Darcy flow regime, the velocity peaks are located away from the vertical walls and exhibit lower values in comparison to the Darcy flow regime.

Moreover, Fig. 9 presents the influence of solid volume fraction at Ra_p = 1000, Da = 10^{-4}, and ϕ = 0.4. There seem to be only slight differences between the temperature and velocity profiles due to a change of solid volume fraction, namely, the velocity profile exhibits the highest peak at φ = 0.05. On the other hand, the type of nanofluid does not influence the course of the temperature or velocity profiles, since in Fig. 10, it is obvious that the profiles for different types of added nanoparticles coincide with each other.

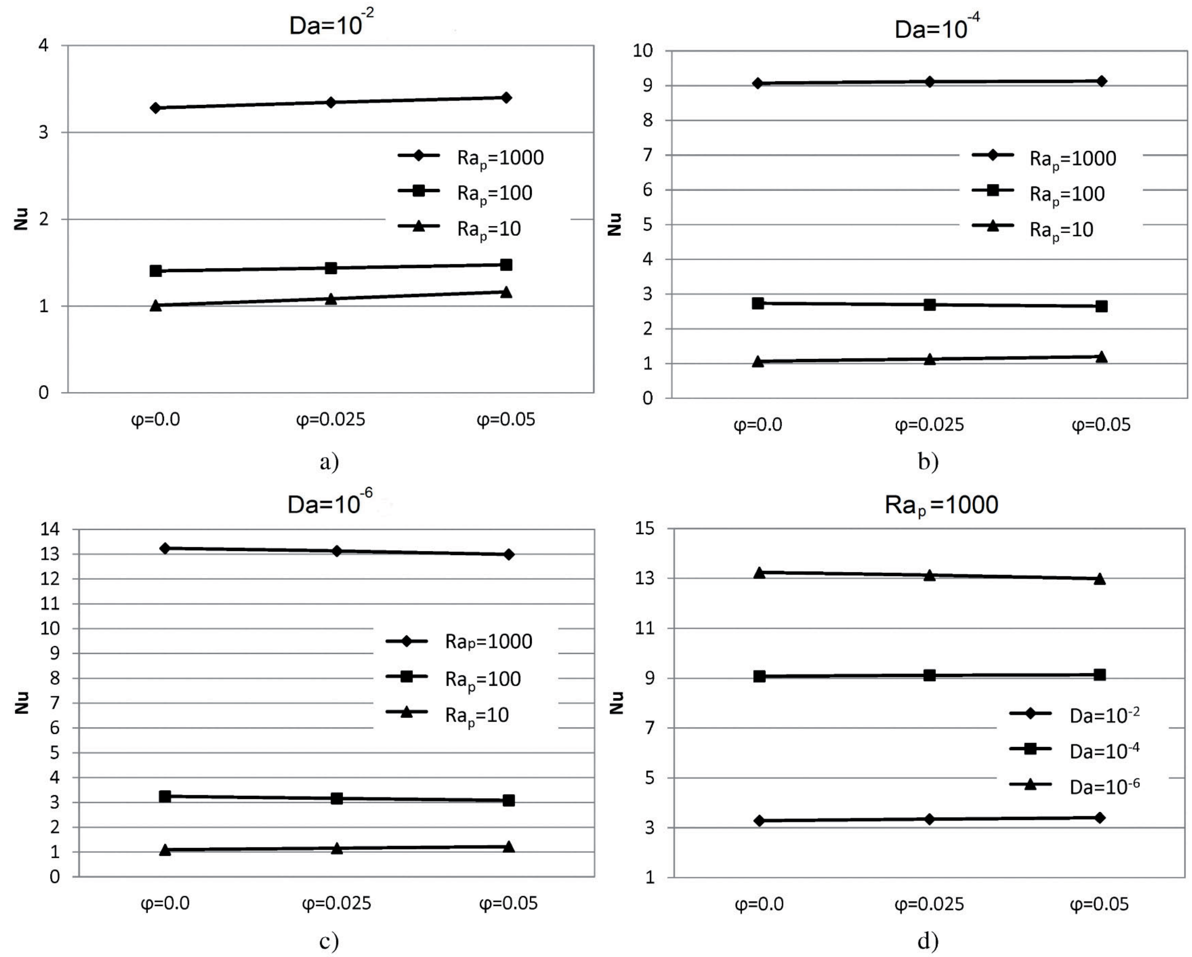

FIG. 4: Average Nu for Cu-water nanofluid depending on solid volume fraction φ for different values of Ra_p and Da: (a) Da = 10^{-2}, (b) Da = 10^{-4}, (c) Da = 10^{-6}, and (d) Ra_p = 1000 (ϕ = 0.4)

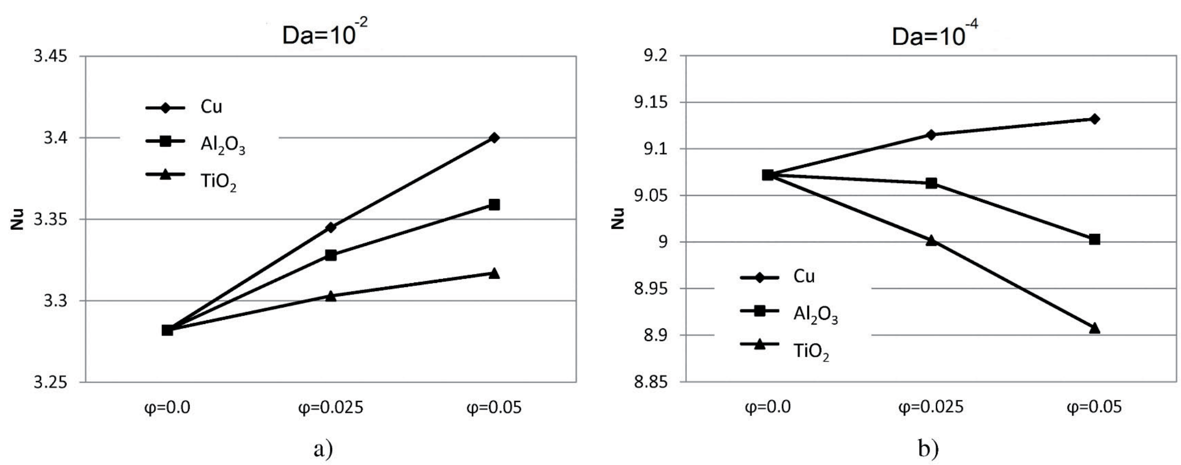

FIG. 5.

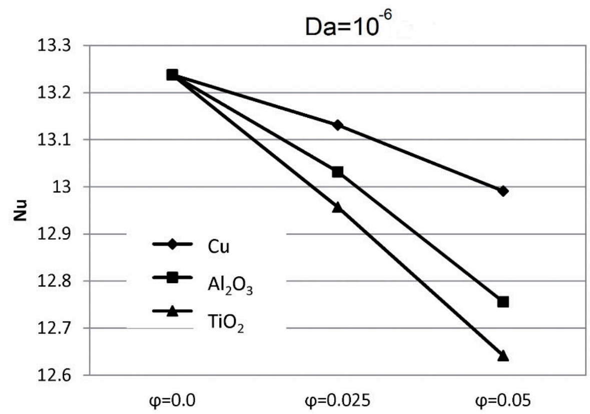

c)

FIG. 5: Average Nu depending on different types of nanoparticles for Ra_p = 1000, various φ and Da: (a) Da = 10^{-2}, (b) Da = 10^{-4}, and (c) Da = 10^{-6} (ϕ = 0.4)

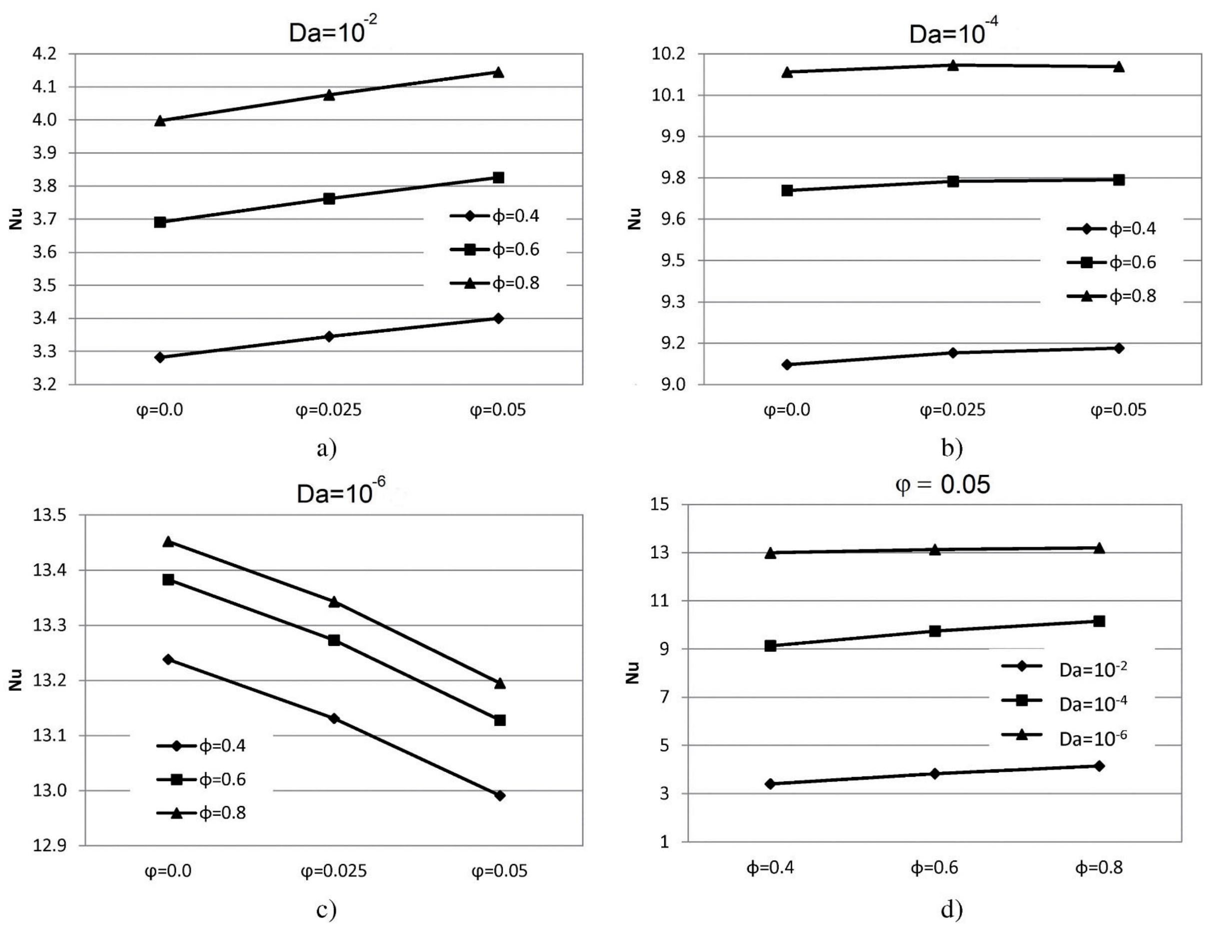

FIG. 6: Average Nu for Cu-water nanofluid depending on porosity ϕ for Ra_p = 1000 and different values of φ and Da: (a) Da = 10^{-2}, (b) Da = 10^{-4}, (c) Da = 10^{-6}, and (d) φ = 0.05

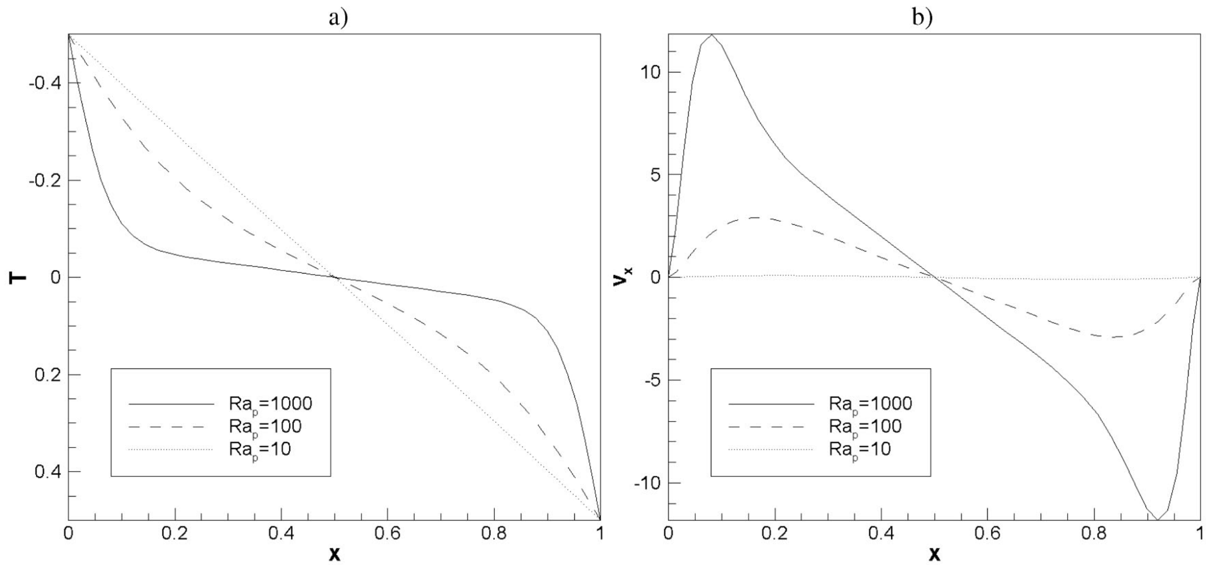

FIG. 7: (a) Temperature and (b) vertical velocity profiles at the horizontal midsection of a cavity for different Ra_p at $\phi = 0.4$ and $\varphi = 0.05$

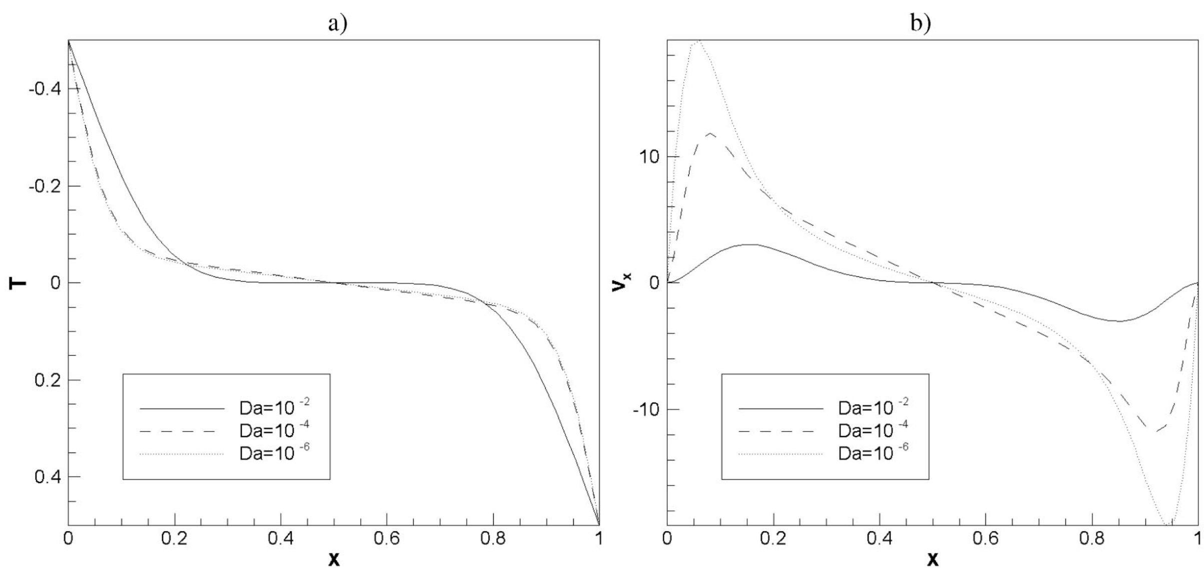

FIG. 8: (a) Temperature and (b) vertical velocity profiles at the horizontal midsection of a cavity for different Da at $\phi = 0.4$ and $\varphi = 0.05$

6. SUMMARY

Numerical analysis of natural convection in a two-dimensional cavity fully filled with nanofluid-saturated porous media has been carried out using the boundary element method. A single-phase mathematical model was used, assuming that the concentration of nanoparticles is low (up to 5%) and that the nanoparticles behave in the same way as the water molecules. The conservation of momentum is described with the Brinkman–Forchheimer momentum equation,

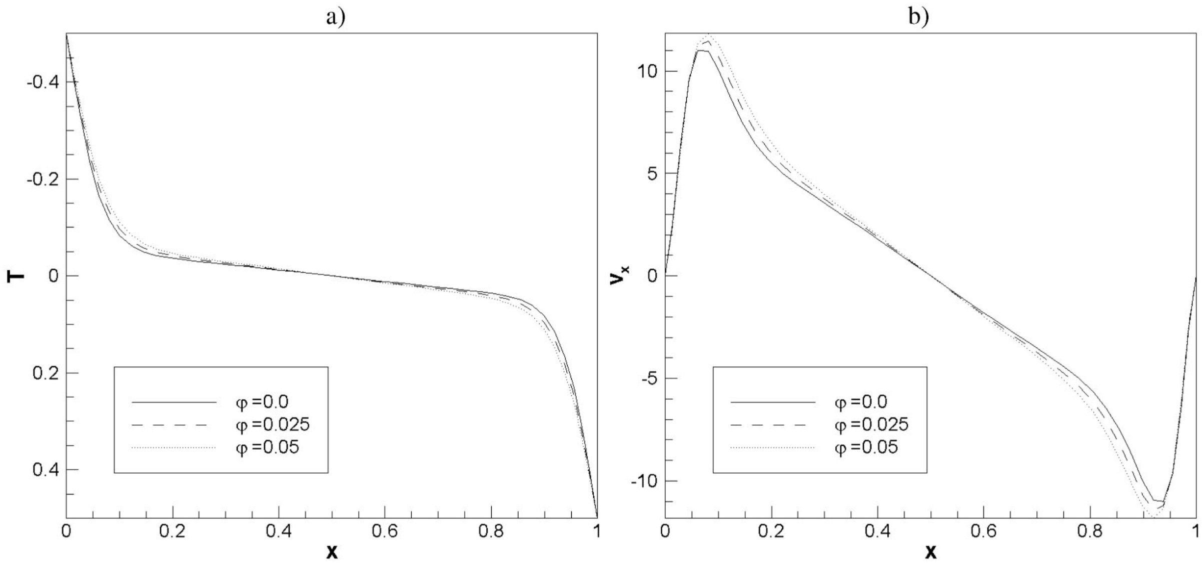

FIG. 9: (a) Temperature and (b) vertical velocity profiles at the horizontal midsection of a cavity for different φ at Ra_p = 1000 and Da = 10^{-4}

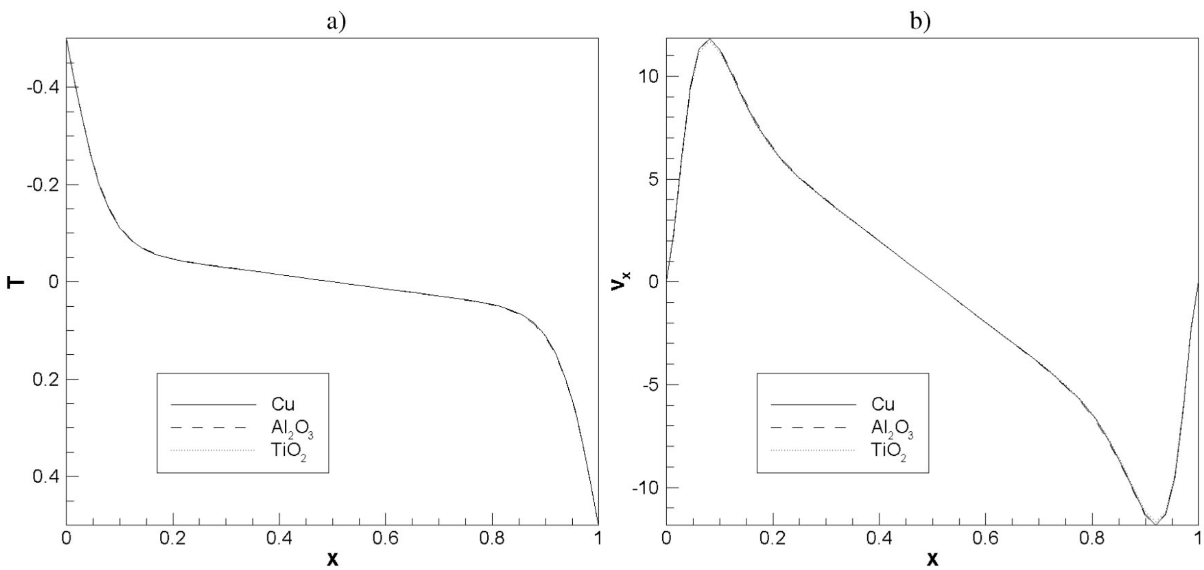

FIG. 10: (a) Temperature and (b) vertical velocity profiles at the horizontal midsection of a cavity for different type of nanofluid at Ra_p = 1000 and Da = 10^{-4}

where the inertial effects are taken into account. The numerical procedure is based on the combination of the single- and subdomain boundary element method, which solves the velocity–vorticity formulation of governing equations. The proposed numerical code was validated by a comparison of present results with the available results from the literature for a wide range of governing parameters. Furthermore, the influence of different types of added nanoparticles into the base fluid on possible heat transfer enhancement was investigated, focusing on the volume fraction of nanoparticles as well as different porous media properties.

The addition of nanoparticles results in higher heat conductivity of the fluid, but it suppresses the natural convection phenomena in general. In the case of the non-Darcy regime (high values of Da), the influence of the Brinkman viscous term in the momentum equation is significant, and the overall heat transfer through a nanofluid-saturated porous cavity is higher in comparison to pure fluid. With a decrease of Da number, the model approaches the Darcy regime, and the overall heat transfer decreases with addition of nanoparticles. When comparing different types of added nanoparticles, the Cu nanoparticles seem to be the most efficient for heat transfer enhancement.

REFERENCES

Abu-Nada, E., Masoud, Z., Oztop, H.F., and Campo, A., Effect of nanofluid variable properties on natural convection in enclosures, *Int. J. Thermal Sci.*, vol. **49**, pp. 479–491, 2010.

Bear, J., *Dynamics of Fluids in Porous Media*, New York, NY: Dover, 1972.

Bourantas, G.C., Skouras, E.D., Loukopoulos, V.C., and Burganos, V.N., Heat transfer and natural convection of nanofluids in porous media, *Eur. J. Mech. B*, vol. **43**, pp. 45–56, 2014.

Brinkman, H.C., The viscosity of concentrated suspensions and solutions, *J. Chem. Phys.*, vol. **20**, pp. 571–581, 1952.

Buongiorno, J., Convective transport in nanofluids, *J. Heat. Transfer*, vol. **128**, pp. 240–250, 2006.

Celli, M., Non-homogeneous model for a side heated square cavity filled with a nanofluid, *Int. J. Heat Fluid Flow*, vol. **44**, pp. 327–335, 2013.

Choi, S.U.S. and Eastman, J.A., Enhancing thermal conductivity of fluids with nanoparticles, *Proc. ASME Int. Mech. Eng. Congress Exposition*, 1995.

Ergun, S., Fluid flow through packed columns, *Chem. Eng. Prog.*, vol. **48**, pp. 89–94, 1952.

Ghalambaz, M., Sheremet, M.A., and Pop, I., Free convection in a parallelogrammic porous cavity filled with nanofluid using Tiwari and Das' nanofluid model, *PLoS ONE*, vol. **10**, no. 5, e0126486, 2015. DOI: 10.1371/journal.pone.0126486

Groşan, T., Revnic, C., Pop, I., and Ingham, D.B., Free convection heat transfer in a square cavity filled with a porous medium saturated by a nanofluid, *Int. J. Heat Mass Transfer*, vol. **87**, pp. 36–41, 2015.

Haddad, Z., Oztop, H.F., Abu-Nada, E., and Mataoui, A., A review on natural convective heat transfer of nanofluids, *Renew. Sust. Energ. Rev.*, vol. **16**, pp. 5363–5378, 2012.

Kakaç, S. and Pramuanjaroenkij, A., Review of convective heat transfer enhancement with nanofluids, *Int. J. Heat Mass Transfer*, vol. **52**, pp. 3187–3196, 2009.

Kramer, J., Ravnik, J., Jecl, R., and Škerget, L., Simulation of 3D flow in porous media by boundary element method, *Eng. Anal. Bound. Elem.*, vol. **35**, pp. 1256–1264, 2011.

Kramer, J., Ravnik, J., Jecl, R., and Škerget, L., Three-dimensional double-diffusive natural convection with opposing buoyancy effects in porous enclosure by boundary element method, *Int. J. Comput. Methods Exper. Measure.*, vol. **1**, pp. 103–115, 2013.

Kuznetsov, A.V., Nanofluid bioconvection in a horizontal fluid-saturated porous layer, *J. Porous Media*, vol. **15**, no. 1, pp. 11–27, 2012a.

Kuznetsov, A.V., Nanofluid bioconvection in porous media: Qxytactic microorganisms, *J. Porous Media*, vol. **15**, no. 3, pp. 233–248, 2012b.

Kuznetsov, A.V. and Nield, D.A., The effect of local thermal nonequilibrium on the onset of convection in a porous medium layer saturated by a nanofluid: Brinkman model, *J. Porous Media*, vol. **14**, no. 4, pp. 285–293, 2011.

Lauriat, G. and Prasad, V., Non-Darcian effects on natural convection in a vertical porous enclosure, *Int. J. Heat Mass Transfer*, vol. **32**, pp. 2135–2148, 1989.

Mahdi, R.A., Mohammed, H.A., Munisamy, K.M., and Saeid, N.H., Review of convection heat transfer and fluid flow in porous media with nanofluid, *Renew. Sust. Energ. Rev.*, vol. **41**, pp. 715–734, 2015.

Mansour, M.A., Ahmed, S.E., and Bakier, M.A.Y., Free convection in h-shaped enclosures filled with a porous medium saturated with nanofluids with mounted heaters on the vertical walls, *Spec. Topics Rev. Porous Media*, vol. **4**, no. 4, pp. 287–297, 2013.

Mittal, N., Manoj, V., Kumar, D.S., and Satheesh, A., Numerical simulation of mixed convection in a porous medium filled with water/Al_2O_3 nanofluid, *Heat Transfer Asian Res.*, vol. **42**, pp. 46–59, 2013.

Muthtamilselvan, M., Kandaswamy, P., and Lee, J., Heat transfer enhancement of copper-water nanofluids in a lid-driven enclosure, *Commun. Nonlinear Sci.*, vol. **15**, pp. 1501–1510, 2010.

Nguyen, M.T., Aly, A.M., and Lee, S.W., Natural convection in a non-Darcy porous cavity filled with Cu-water nanofluid using the characteristic-based split procedure in finite-element method, *Numer. Heat Transfer A*, vol. **67**, pp. 224–247, 2015.

Nield, D.A. and Bejan, A., *Convection in Porous Media*, (4th ed.), New York, NY: Springer, 2013.

Nithiarasu, P., Seetharamu, K.N., and Sundararajan, T., Natural convective heat transfer in a fluid saturated variable porosity medium, *Int. J. Heat Mass Transfer*, vol. **40**, pp. 3955–3967, 1997.

Oztop, H.F. and Abu-Nada, E., Numerical study of natural convection in partially heated rectangular enclosures filled with nanofluids, *Int. J. Heat Fluid Flow*, vol. **29**, pp. 1326–1336, 2008.

Pop, I. and Ingham, D.B., *Convective Heat Transfer: Mathematical and Computational Viscous Fluids and Porous Media*, Oxford, UK: Pergamon, 2001.

Prabhat, N., Buongiorno, J., and Hu, L.W., Convective heat transfer enhancement in nanofluids: Real anomaly or analysis artifact?, *J. Nanofluids*, vol. **1**, pp. 55–62, 2012.

Ramšak, M., Škerget, L., Hriberšek, M., and Žunič, Z., A multidomain boundary element method for unsteady laminar flow using stream function vorticity equations, *Eng. Anal. Bound. Elem.*, vol. **29**, pp. 1–14, 2005.

Ravnik, J., Škerget, L., and Žunič, Z., Velocity-vorticity formulation for 3D natural convection in an inclined enclosure by BEM, *Int. J. Heat Mass Transfer*, vol. **51**, pp. 4517–4527, 2008.

Ravnik, J., Škerget, L., and Žunič, Z., Combined single domain and subdomain BEM for 3D laminar viscous flow, *Eng. Anal. Bound. Elem.*, vol. **33**, pp. 420–424, 2009.

Ravnik, J., Škerget, L., and Hriberšek, M., Analysis of three-dimensional natural convection of nanofluids by BEM, *Eng. Anal. Bound. Elem.*, vol. **34**, pp. 1018–1030, 2010.

Saleh, H. and Hashim, I., Natural convection from a cylinder in square porous enclosure filled with nanofluids, *J. Porous Media*, vol. **18**, no. 4, pp. 559–567, 2015.

Sheikhzadeh, G.A. and Nazari, S., Numerical study of natural convection in a square cavity filled with a porous medium saturated with nanofluid, *Transport Phenomena Nano Micro Scales*, vol. **1**, pp. 138–146, 2013.

Sheremet, M.A. and Pop, I., Conjugate natural convection in a square porous cavity filled by a nanofluid using Buongiorno's mathematical model, *Int. J. Heat Mass Transfer*, vol. **79**, pp. 137–145, 2014.

Sheremet, M.A., Grosan, T., and Pop, O., Free convection in a square cavity filled with a porous medium saturated by nanofluid using Tiwari and Das' nanofluid model, *Transport Porous Media*, vol. **106**, pp. 595–610, 2015.

Škerget, L. and Jecl, R., Compressible fluid dynamics in porous media by the boundary element method, in *Emerging Technologies and Techniques in Porous Media*, D.B. Ingham, A. Bejan, E. Mamut, and I. Pop, (Eds.), New York, NY: Kluwer Academic, 2003.

Tiwari, R.K. and Das, M.K., Heat transfer augmentation in a two-sided lid driven differentially heated square cavity utilizing nanofluids, *Int. J. Heat Mass Transfer*, vol. **50**, pp. 2002–2018, 2007.

Vafai, K. (Ed.), *Handbook of Porous Media*, New York, NY: Taylor & Francis, 2005.

Wasp, F.J., *Solid-Liquid Slurry Pipeline Transportation*, Berlin, Germany: Trans. Tech., 1977.

Yasin, M.H.M., Ishak, A., and Pop, I., Steady double-diffusive mixed convection boundary layer flow past a vertical flat plate embedded in a porous medium filled by a nanofluid using Buongiorno's model, *J. Porous Media*, vol. **19**, no. 4, pp. 331–338, 2016.

Žunič, Z., Hriberšek, M., Škerget, L., and Ravnik, J., 3-D boundary element-finite element method for velocity-vorticity formulation of the Navier-Stokes equations, *Eng. Anal. Bound. Elem.*, vol. **31**, pp. 259–266, 2007.